JOURNAL OF SOLID STATE CHEMISTRY **138,** 350–360 (1998)
ARTICLE NO. SC977545

# Structure of $Sn(ND_3)_2F_4$—A Molecular Precursor for the Synthesis of Nitride Fluorides

Pat Woodward and Tom Vogt[1]

*Physics Department, Brookhaven National Laboratory, Upton, New York 11973*

and

Wolfram Weber and Eberhard Schweda

*Institut für anorganische Chemie, Universität Tübingen, Auf der Morgenstelle 18, 72076 Tübingen, Germany*

Received March 31, 1997; in revised form July 7, 1997; accepted July 15, 1997

DEDICATED TO PROFESSOR J. STRÄHLE ON THE OCCASION OF HIS 60TH BIRTHDAY

**The molecular and crystal structure of $Sn(ND_3)_2F_4$ has been determined at room temperature using high resolution neutron powder diffraction. The compound crystallizes in a monoclinic unit cell containing two formula units with $a = 7.7673(7)$ Å, $b = 6.2765(5)$ Å, $c = 5.1708(4)$ Å, $\beta = 102.871(5)^\circ$, and space-group $P2_1/n$. The structure consists of isolated tin-centered octahedra with ammonia groups in *trans* configuration. The intramolecular stability of this compound has been investigated using Hückel molecular orbital calculations. Compared to $Si(NH_3)_2F_4$, the metal–nitrogen bonding interaction is found to be stronger, while the metal–fluorine bond is weaker in $Sn(ND_3)_2F_4$. Due to a different hydrogen bonding network the intermolecular orientation and packing of the octahedral $M(NH_3)_2F_4$ molecules in $Sn(ND_3)_2F_4$ is different from the arrangement observed in $Si(NH_3)_2F_4$. The implications for the use of these compounds as molecular precursors for the synthesis of SiNF and SnNF are discussed.** 

***Key Words*: synthesis; nitride fluorides; crystal structures; neutron diffraction; infrared spectroscopy, Hückel calculations.**

## INTRODUCTION

Reactions in traditional solid state synthesis are thermodynamically controlled. In most cases this results in the complete structural modification of the starting materials and does not, as in organic synthesis, allow for kinetic control involving only the rearrangement of a few bonds. The concept of a functional group does not exist in solid state synthesis and the difficulties of a rational and strategic approach are furthermore hampered by large transport distances and small diffusion coefficients, which generally necessitate high reaction temperatures. In recent years low temperature synthesis involving molecular precursors ("chimie douce") has started to alter this picture (1). Focusing attention on reactions of molecular precursors containing building blocks of the target solid is even more important in attempting to synthesize nonoxide materials. Up to now the tailoring of optical, magnetic, or electrical properties (e.g., superconductivity) has been achieved via substitution of the cations. In contrast, modification of the anion sublattice is generally more difficult and thus less frequently attempted. Nitride halides are an interesting family of compounds where two group VI anions are formally replaced by a $N^{3-}$ and a group VII anion. Nitride halides and particulary the nitride fluorides, for which Andersson (2) coined the term pseudooxides, are a relatively unexplored class of compounds (3). The distinction of the nitride flourides from the remainder of the nitride halides is based on variations of the size and electronic properties of the two anions. In a very simple picture, size and electronic properties can be contrasted, using pseudopotential core radii sums ($R = rs + rp$) in Å and Matynov–Batsanov electronegativities $X$ in $(\text{eV})^{1/2}$ (4). Nitrogen ($R = 0.54$ Å, $X = 2.85\,(\text{eV})^{1/2}$) and flourine ($R = 0.405$ Å, $X = 3.78\,(\text{eV})^{1/2}$)have rather similar anion sizes ($\Delta R = 0.135$ Å) but different electronegativities ($\Delta X = 0.93\,(\text{eV})^{1/2}$). On the other hand, the anion pairs in nitride chlorides ($\Delta R = 0.47$ Å, $\Delta X = 0.13\,(\text{eV})^{1/2}$), nitride bromides ($\Delta R = 0.66$ Å, $\Delta X = 0.02\,(\text{eV})^{1/2}$), and nitride iodides ($\Delta R = 1.045$ Å, $\Delta X = 0.09\,(\text{eV})^{1/2}$) have significantly different radii but rather similar electronegativities. The electronegativity and size differences lead to synthetic challenges, especially in the case of nitride fluorides. The quest for materials such

[1]To whom correspondence should be addressed.



0022-4596/98 $25.00

as SiNF which could possibly be "alloyed" with $SiO_2$ has intensified (5). The synthesis route currently favored is the ammonolysis of molecular ammonium metal halide complexes.

If we limit ourselves to the ammonolysis of main group IV ammonium metal fluoride salts to nitride fluorides we observe the following reaction path:

$$\underset{\text{(I)}}{(NH_4)_2MF_6} \rightarrow \underset{\text{(II)}}{(NH_4)MF_5(NH_3)} \rightarrow \underset{\text{(III)}}{M(NH_3)_2F_4} \rightarrow$$

$$\underset{\text{(IV)}}{M(NH_2)_2F_2} \rightarrow \underset{\text{(V)}}{MNF}.$$

The reaction progresses from hexacoordinated molecular complexes (I), (II), and (III) via HF abstractions to an extended one-dimensional systems (IV) with edge-sharing octahedral chains and finally to pseudooxides (V) with three dimensional network structures. The important condensation step occurring when going from (III) to (IV) will depend on the stability of the extended system (IV) with respect to the molecular stability of (III), as well as the ease with which the hydrogen bonding network in (III) can be modified during successive HF abstractions.

Weber and Schweda (6, 7) have investigated the reaction paths of the tin and germanium ammonium hexafluorometal complexes and established the existences of (I), (II), (III), and (IV) for $M = Sn$ using *in situ* $X$-ray diffraction techniques. For $M = Ge$ they established the existence of (III). Plitzko and Meyer (5) confirmed the existence of (II) and (III) for $M = Si$. We have determined the structure of (III) in the tin system using high resolution neutron powder diffraction. This allows us to compare the molecular and crystal structures for the tin and silicon complex (III). The understanding of the hydrogen bonding network in the crystal structure is crucial since it will have to be altered to proceed with the ammonolysis. Furthermore, molecular

**TABLE 1**
**Infrared Absorption Frequencies and Band Assignments for $Sn(NH_3)F_2$ and $Sn(ND_3)F_4$**

| $Sn(NH_3)_2F_4$ | | $Sn(ND_3)_2F_4$ | | | |
|---|---|---|---|---|---|
| $\nu$ ($cm^{-1}$) | Intensity | $\nu$ ($cm^{-1}$) | Intensity | Assignment | $\nu(H)/\nu(D)$ |
| 3299 | vs | 2466 | vs | $\nu_{as}NH_3$ | 1.34 |
| 3200 | w | 2332 | m | $\nu_sNH_3$ | 1.37 |
| 1656 | m | 1250 | w | $\delta_{as}NH_3$ | 1.32 |
| 1529 | m | 1130 | vw | $\delta_{as}NH_3$ | 1.35 |
| 1309 | vs | 1010 | vs | $\delta_sNH_3$ | 1.30 |
| 804 | vs | 615 | m | $\delta_r$Sn–N–H | 1.31 |
| 550 | vs | 549 | vs | $\nu$ Sn–$F_{eq}$ | 1.00 |
| 505 | s | 473 | m | $\nu$ Sn–$F_{ax}$ | 1.07 |

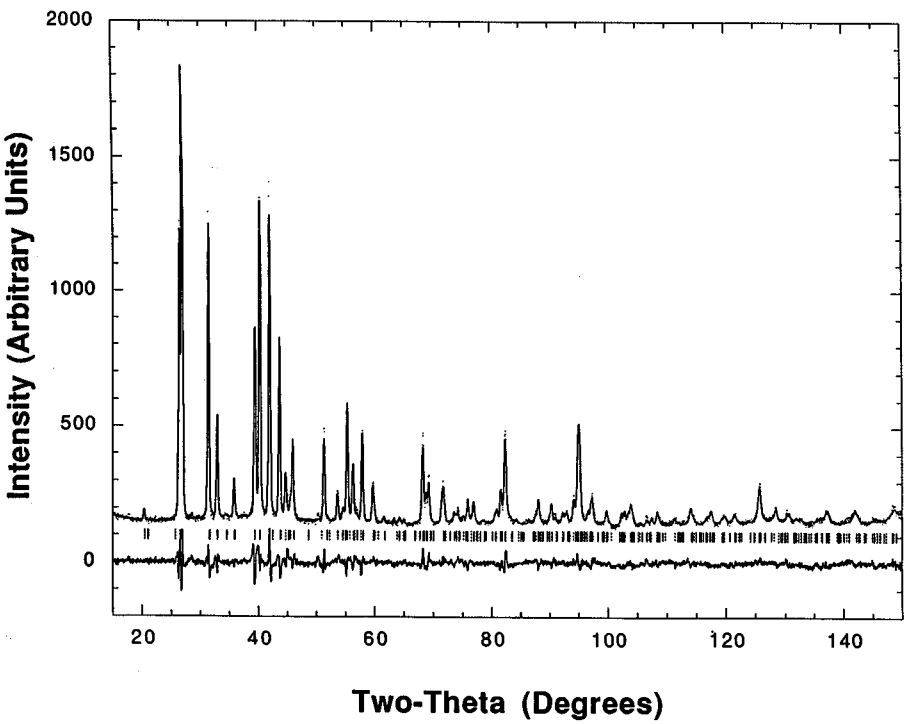


**FIG. 1.** The observed, calcualted, and difference patterns for the neutron diffraction pattern used in the Rietveld refinements. The observed data points are represented by dots while the calculated and difference patterns are represented by solid lines. The possible peak positions are marked with vertical tick marks.

**TABLE 2**
**Rietveld Refinement Parameters**

| Refinement parameters for $SnF_4(ND_3)_2$ | |
|---|---|
| $R_{wp}$ | 5.30% |
| $R_p$ | 4.15% |
| $R(F^2)$ | 9.44% |
| $\chi^2$ | 0.56 |
| Space group | $P2_1/n$ |
| $Z$ | 2 |
| $a$ | 7.7673(7) Å |
| $b$ | 6.2764(5) Å |
| $c$ | 5.1708(4) Å |
| $\beta$ | 102.871(5)° |
| Cell volume | 248.91(5) Å$^3$ |
| 2Θ range | 15–150° |
| # of data points | 2700 |
| # of Bragg peaks | 298 |
| # of variables | 55 |
| # of strucutral variables | 40 |

orbital calculations using the Hückel method provide us with an understanding of the intramolecular stability of these complexes. The intriguing question posed by Plitzko and Meyer (5), why the extended systems (IV) and (V) are not observed when $M$ = Si, is examined by comparing the molecular, crystalline, and electronic structures of the tin and silicon complexes (III).

## EXPERIMENTAL SECTION

### *Synthesis*

The ammonolysis reaction of $(NH_4)_2SnF_6$ to $Sn(NH_3)_2F_4$ was carried out as described earlier (6, 7). Hydrogen was substituted by deuterium in $(NH_4)_2SnF_6$ by exchanging consecutively with $ND_3$ (Cambridge Isotope Laboratories Inc.). The degree of substitution was monitored every 6 h by X-ray diffraction and IR spectroscopy. A series of IR spectra reveal that after 6 h almost all the hydrogen was replaced by deuterium. The strong absorption at 3372 cm$^{-1}$, which is assigned to the N–H stretching vibration, is left with very little intensity. The N–D stretching vibration appears at 2453 cm$^{-1}$. The reaction to $Sn(ND_3)_2F_4$ is completed after 56 h. Attempts to directly deuterate $Sn(NH_3)_2F_4$ have not been successful. Important absorption bands of $Sn(NH_3)_2F_4$ and $Sn(ND_3)_2F_4$, respectively, are listed in Table 1.

**TABLE 3**
**Atomic Fractional Coordinates and Isotropic Thermal Parameters**

| Atom | Site | $x$ | $y$ | $z$ | $B_{iso}$ |
|---|---|---|---|---|---|
| Sn | 2a | 0 | 0 | 0 | 2.0(2) |
| F(1) | 4e | − 0.075(1) | − 0.1893(7) | 0.263(1) | 2.8(2) |
| F(2) | 4e | 0.2384(9) | − 0.0008(9) | 0.231(1) | 2.1(1) |
| N | 4e | − 0.065(1) | 0.2684(7) | 0.199(1) | 2.3(1) |
| D(1) | 4e | − 0.069(2) | 0.236(1) | 0.382(2) | |
| D(2) | 4e | 0.035(1) | 0.377(1) | 0.228(2) | |
| D(3) | 4e | − 0.156(1) | 0.349(2) | 0.111(3) | |

**TABLE 4**
**Anisotropic Thermal Parameters for the Deuterium Atoms**

| Atom | $U_{11}$ | $U_{22}$ | $U_{33}$ | $U_{12}$ | $U_{13}$ | $U_{23}$ | $B_{eq}$ |
|---|---|---|---|---|---|---|---|
| D(1) | 4.8(6) | 3.7(6) | 23(2) | 2.9(5) | − 4.8(9) | − 6.3(7) | 9.0 |
| D(2) | 12(1) | 5.2(6) | 9.3(9) | − 1.7(6) | 7.6(9) | − 0.6(5) | 6.1 |
| D(3) | 7.9(8) | 4.7(6) | 8.4(7) | − 0.6(5) | 0.1(5) | − 3.4(4) | 5.5 |

### *High-Resolution Neutron Powder Diffraction*

A high-resolution neutron powder diffraction pattern was obtained on the high-resolution neutron powder diffractometer located on beamline H1A at the High Flux Beam Reactor at Brookhaven National Laboratory. A 30 cm tall focusing monochromator composed of 24 Ge(115) composites at a take-off angle of 120° provides a wavelength of 1.8857 Å. The design of this wafer-based monochromator is described elsewhere (8). The detector bank is equipped with 64 $^3$He detectors separated by 2.5° in 2$\theta$. In front of each

**TABLE 5**
**Selected Bond Distances and Angles**

| Bond distances (Å) | | Bond angles (°) | |
|---|---|---|---|
| Sn–F(1) | 1.994(5) | N–Sn–F(1) | 89.9(2) |
| Sn–F(2) | 1.986(7) | N–Sn–F(2) | 89.3(4) |
| Sn–N | 2.096(4) | F(1)–Sn–F(2) | 88.4(4) |
| N–D(1) | 0.91(1) | Sn–N–D(1) | 116.9(9) |
| N–D(2) | 0.98(1) | Sn–N–D(2) | 111.8(6) |
| N–D(3) | 1.03(1) | Sn–N–D(3) | 109.8(7) |
| | | D(1)–N–D(2) | 114.8(1) |
| D(1)–F(2) | 2.18(1) | D(1)–N–D(3) | 101.4(1) |
| D(1)–F(1) | 2.36(2) | D(2)–N–D(3) | 100.0(1) |
| D(2)–F(1) | 1.95(2) | | |
| D(2)–F(2) | 3.03(1) | | |
| D(3)–F(2) | 1.91(1) | | |
| D(3)–F(1) | 2.84(2) | | |

**FIG. 3.** An extended view, clearly showing the intermolecular packing, in (a) $Sn(ND_3)_2F_4$ and (b) $Si(NH_3)_2F_4$. Both views show a $c$-axis projection, with the $b$ axis running verically and the $a$ axis horizontally within the plane of the paper. The tin ions are represented by yellow spheres, the silicon ions by red spheres, the fluorine ions by green spheres, the nitrogen ions by blue spheres, and the hydrogen ions by white spheres. In part (a) the hydrogen bonding interactions are depicted by dotted white lines.

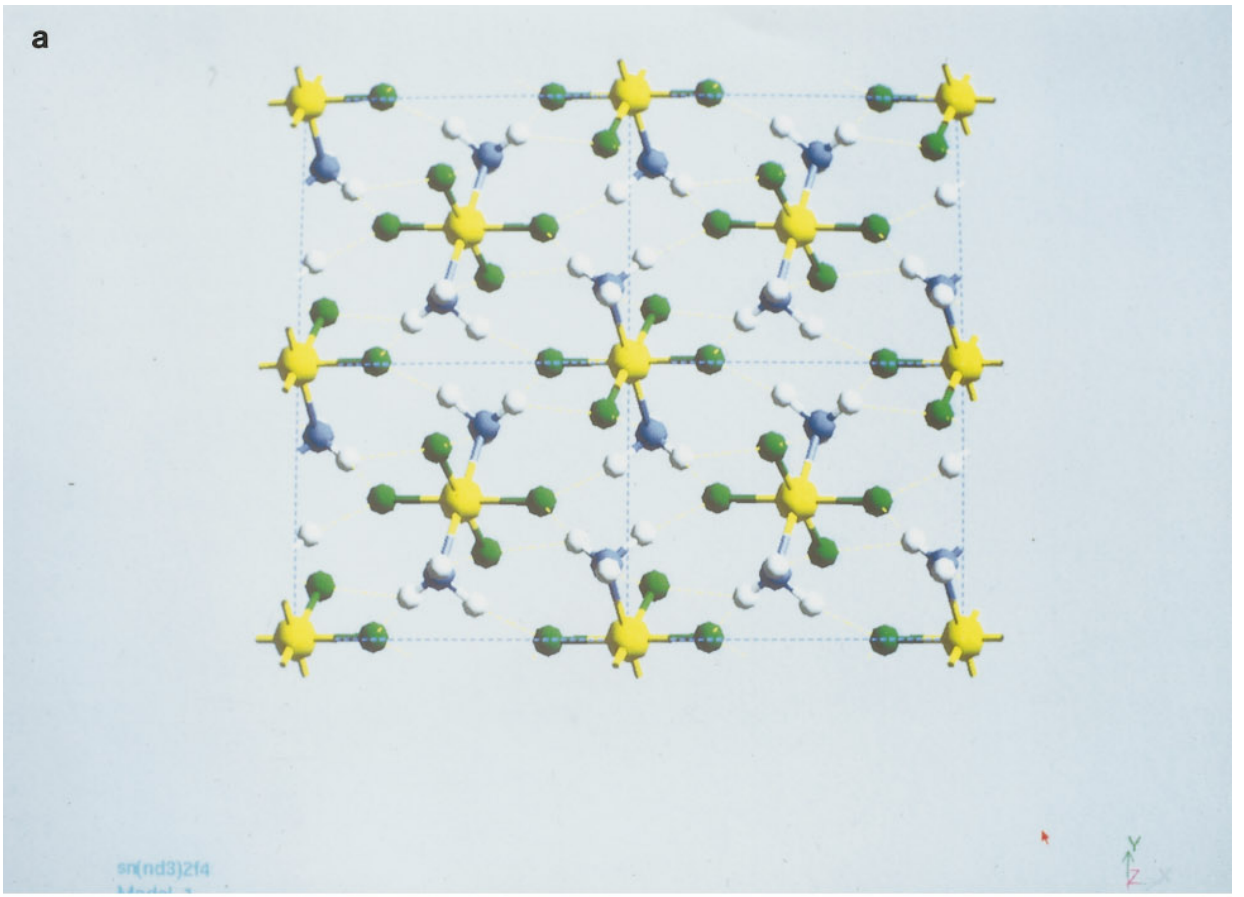
a
sn(nd3)2f4

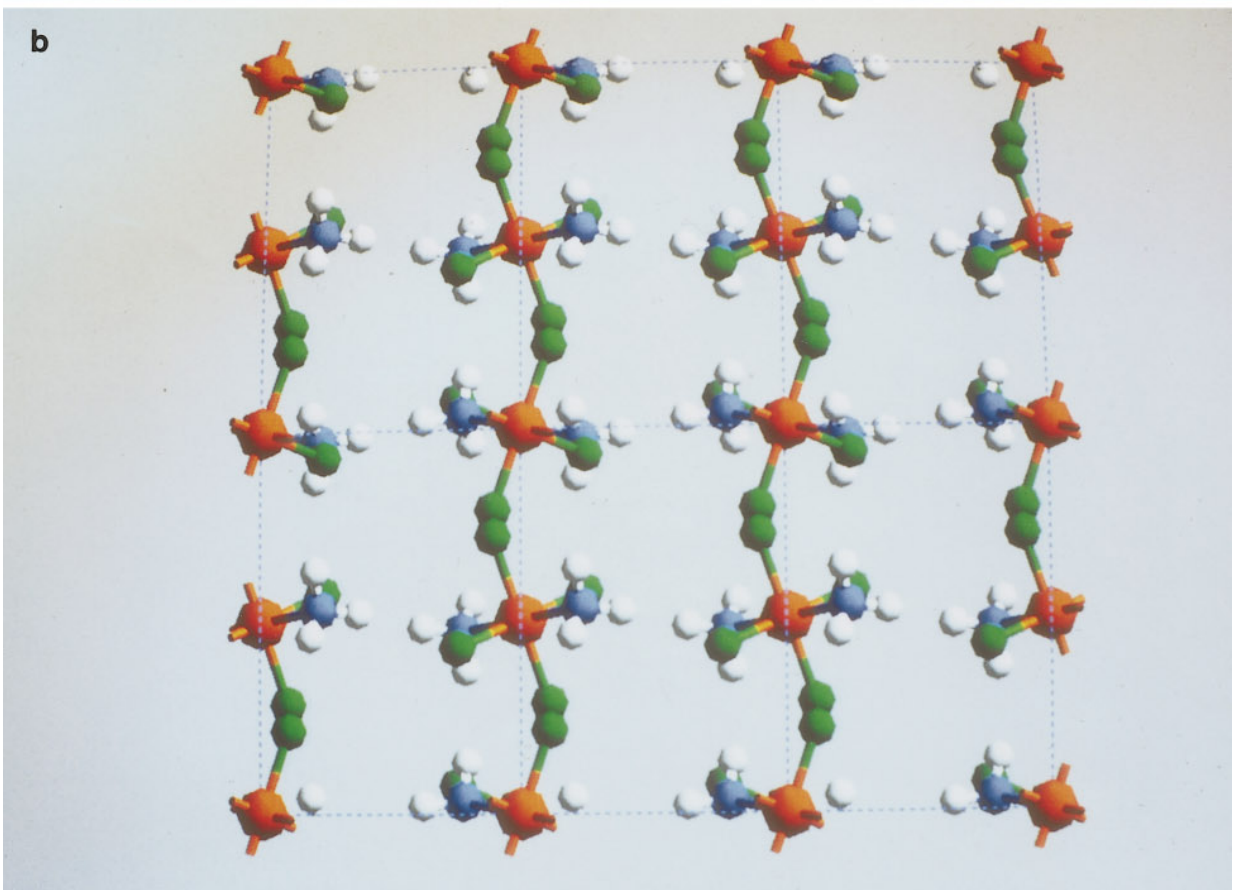
b

**TABLE 6**
**Exponents $\zeta_i$ and Valence Shell Ionization Potentials $H_{ii}$ of Slater-Type Orbitals $\chi_i$ Used in the Extended Hückel Calculations**

| Atom | $\chi_i$ | $H_{ii}$ (eV) | $\zeta_i$ |
|---|---|---|---|
| Sn | 5*s* | − 16.60 | 2.12 |
| Sn | 5*p* | − 8.32 | 1.82 |
| Si | 3*s* | − 17.30 | 1.383 |
| Si | 3*p* | − 9.20 | 1.383 |
| N | 2*s* | − 26.00 | 1.95 |
| N | 2*p* | − 13.40 | 1.95 |
| F | 2*s* | − 40.00 | 2.425 |
| F | 2*p* | − 18.10 | 2.425 |
| H | 1*s* | − 13.60 | 1.3 |

*Note.* For a description of the way in which these parameters are used see Albright, Burdett, and Whangbo (16). For the off-diagonal matrix elements $H^{\text{eff}} = \langle\chi_i|H^{\text{eff}}|\chi_l\rangle$ the weighted formula was used (17).

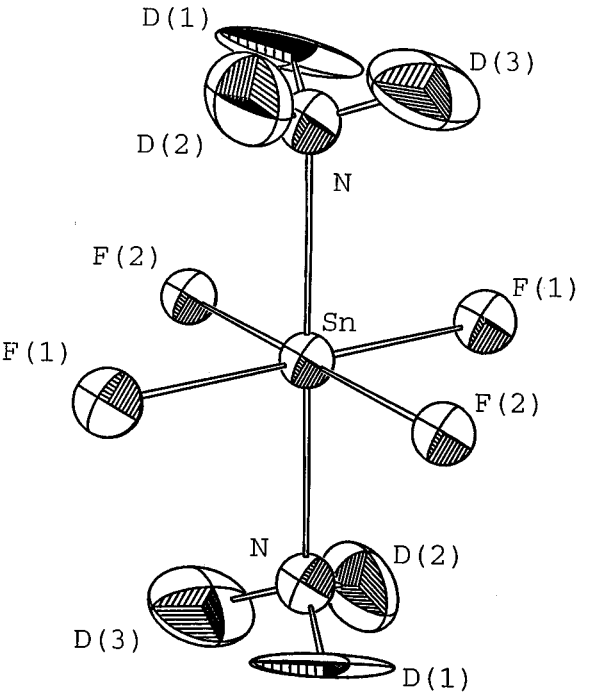


**FIG. 2.** An ORTEP drawing of the $Sn(ND_3)_2F_4$ molecular geometry. Notice that the shape of the thermal ellipsoid associated with the D(1) atom, which is involved in a bifurcated hydrogen bond to fluorine, differs significantly from the D(2) and D(3) thermal ellipsoids. The elongation of this ellipsoid may be indicative of disorder, either static or dynamic, in the orientation of this atom.

detector a 5′ collimator provides tertiary collimation. Primary collimation in front of the monochromator was 11′. No secondary collimation was used. The detector bank was stepped in 0.05 degree steps. Blocks of intensity and position were normalized with respect to detector efficiency and positional errors. The data consisted of 3000 points from 0 to 150° in $2\theta$.

Rietveld refinement of the data was carried out using the GSAS software package (9). Earlier refinements of *X*-ray data (7) indicated two possible unit cells: a C-centered cell with lattice constants $a = 8.404$ Å, $b = 6.278$ Å, $c = 5.178$ Å, $\beta = 114.04°$, Vol = 248.5 Å$^3$, and a body-centered cell with lattice constants $a = 7.87$ Å, $b = 6.28$ Å, $c = 5.17$ Å, $\beta = 10.2.87°$, Vol = 248.9 Å$^3$. Initial refinement attempts using the former cell, in several monoclinic space groups, were not able to produce a satisfactory fit to the observed diffraction pattern. Subsequent use of the auto indexing program TREOR (10), using the first 20 peak positions of the neutron diffraction pattern as input, showed that although the peaks could be indexed using either cell, the systematic absences were consistent with a unit cell metrically equivalent to the body-centered cell, but belonging to space group $P2_1/n$. From the size of the unit cell and the stoichiometry it was inferred that each unit cell contained two isolated, tin-centered octahedra. The observation of a body-centered cell in the X-ray data indicated that the tin atoms were separated by $\frac{1}{2}, \frac{1}{2}, \frac{1}{2}$. In space group $P2_1/n$ this implies that the tin atoms must lie on inversion centers. Based on this information the tin atoms were placed at 0, 0, 0 and $\frac{1}{2}, \frac{1}{2}, \frac{1}{2}$ (Wyckoff site 2a). Furthermore, the inversion center implies a *trans* configuration of the ammonia groups. At this point an ideal rigid body was defined using Sn–F, Sn–N, and N–D distances of 1.97, 2.15, and 0.90 Å, respectively (based on the crystal radii of Shannon (11), ideal bond angles, and $ND_3$ groups in *trans* configuration. The rotation angles of the rigid body about each of the three Cartesian axes were defined, reducing the number of structural variables to 3. Although this approach did not initially give a good fit to the pattern, changing the starting values of the rotation angles several times to avoid local minima soon led to rapid convergence upon the global minimum. Once this occurred the rigid body constraints were removed, with the exception of the ammonia molecules. Subsequently, after several further refinement cycles, all rigid body and soft constraints were removed. Allowing the unrestrained model to minimize with isotropic displacement parameters led to a weighted residual of $R_{\text{wp}} = 6.28\%$. Finally, using anisotropic displacement parameters for the deuterium, the residual $R_{\text{wp}}$ dropped to 5.30%. The observed, calculated and difference patterns are shown in Fig. 1. Refinement parameters are given in Table 2, atomic positions and isotropic displacement parameters in Table 3 and the deuterium anisotropic displacement parameters in Table 4. Table 5 lists selected bond distances and angles.

## *Extended Hückel Calculations*

Molecular orbital calculations were performed using the program CAESAR developed for a Windows environment, written by Jinqing Ren and Myung-Hwan Whangbo. The

**TABLE 7**
**Results of Bond Valence Calculations**

| Bond | $SnF_4(ND_3)_2$ | $SiF_4(NH_3)_2$ |
|---|---|---|
| Sn/Si–F(1) | 0.67 | 0.88 |
| Sn/Si–F(2) | 0.68 | 0.86 |
| Sn/Si–N | 0.93 | 0.63 |
| N–D(1) /H(1) | 0.94 | 1.23 |
| N–D(2) /H(2) | 0.78 | 1.40 |
| N–D(3) /H(3) | 0.68 | 1.19 |
| Sn/Si total | 4.54 | 4.72 |
| F total (Ave) | 0.68 | 0.87 |
| N total | 3.32 | 4.45 |

*Note.* All calculations were done using the program VALENCE (18). Bond distances for $SiF_4(NH_3)_2$ were taken from Plitzko and Meyer (5).

calculations are based on the extended Hückel method (12–15). Calculations were performed on isolated molecules of both $Sn(NH_3)_2F_4$ and $Si(NH_3)_2F_4$, and because the distortions in the structures are very small, idealized molecules of the $D_{4h}$ symmetry (neglecting the hydrogen) were assumed. The Sn–F, Sn–N, Si–F, and Si–N bond distances were taken to be 2.00 Å, 2.10 Å, 1.67 Å and 1.90 Å respectively. All N–M–F and F–M–F bond angles were fixed at 90° and the bond angles around the nitrogen at 109.5° with N–H distances of 0.90 Å for both compounds. The parameters used in our Hückel calculations are listed in Table 6.

## RESULTS

### *Molecular and Crystal Structure of $Sn(ND_3)_2F_4$*

The monoclinic unit cell $P2_1/n$ contains two formula units. The tin atoms are located at the origin and $\frac{1}{2}, \frac{1}{2}, \frac{1}{2}$, thus forming a body centered arrangement. They are hexacoordinated by four flourines and two $NH_3$-groups which are in *trans* position with respect to each other (Fig. 2). In a projection down the *c*-axis it can be seen that the orientation of the N–Sn–N axis in the octahedra with respect to the *b*-axis is alternated between the separated columns running along the *a*-axis (Fig. 3a). The orientations of the $Sn(ND_3)_2F_4$ octahedra within the unit cell are a consequence of the hydrogen bonding network. The results of the Rietveld refinement in Tables 3 and 4 reveal that the displacement parameters of D(2) and D(3) are significantly smaller than those observed for D(1). D(1) is involved in a bifurcated hydrogen bond with the adjacent fluorine atoms F(1) and F(2). The distances of 2.18(1)Å to F(2) and 2.36(1) Å to F(1) are longer than the single hydrogen bonds D(2)–F(1) with 1.95(2) Å and D(3) –F(2) with 1.91(1) Å. The N–D(1) bond with 0.91(1) Å is the shortest and strongest of the N–D bonds. The anisotropic displacement parameter (see Fig. 3 and Table 4) of D(1) indicates the likely presence of disorder along the *c*-axis where F(1)–D(1)–F(2) interactions bridge the octahedra centered at $\frac{1}{2}, \frac{1}{2}, \frac{1}{2}$ and the octahedra at 0, 0, 0.

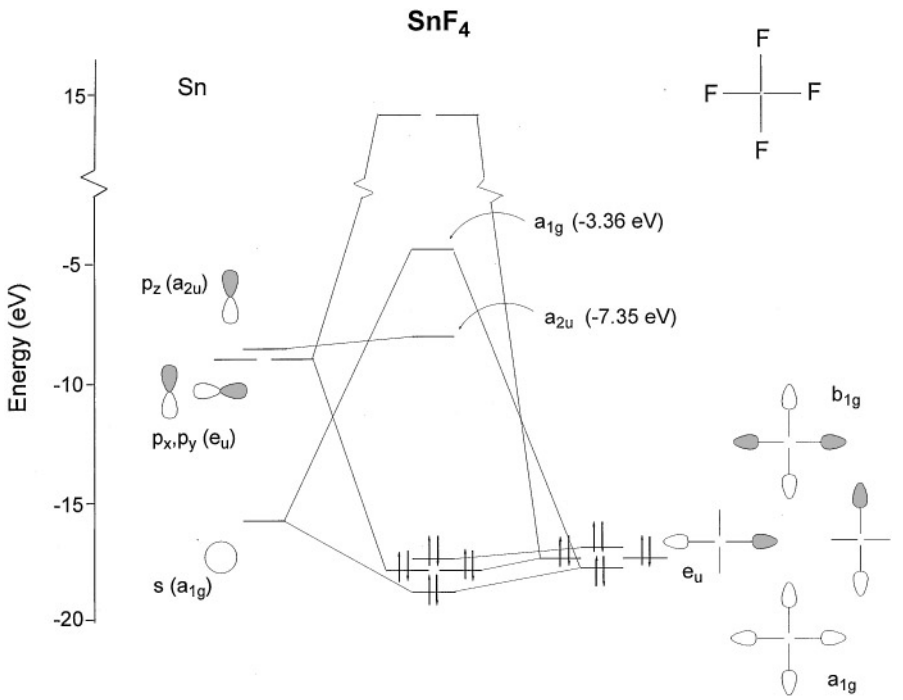


**FIG. 4.** The MO interaction diagram for the hypothetical molecule $SnF_4$. For simplicity the fluorine based orbitals, which are primarily nonbonding in character, have been omitted. The two lowest energy unoccupied orbitals of $a_{2u}$ ( −7.35 eV) and $a_{1g}$ ( −3.36 eV) symmetry are shown in more detail in Fig. 6.

*Bond Valence Calculations*

When the bond valence sums of $Sn(ND_3)_2F_4$ are calculated (Table 7) the overbonding of the tin and nitrogen and the underbonding of the fluorines indicate the covalent bonding character of the tin–nitrogen interaction. The valence sums of the deuterium ions indicate that D(1) satisfies its bonding requirements much better than D(2) and D(3). The individual bond valence contributions to nitrogen reveal that D(1) is involved in the strongest bond followed by tin and D(2) and D(3). It would thus appear to be energetically favorable to break up one of the latter two hydrogen bonds when going from complex (III) to (IV) via HF abstraction. The individual bond valences around tin indicate that the bonds to nitrogen are significantly stronger than the tin–fluorine bonds.

*Structural Comparison to $Si(NH_3)_2F_4$*

The structure of $Si(NH_3)_2F_4$ was solved by Plitzko and Meyer (5) using single crystal X-ray diffraction. This molecular complex of type (III) also crystallizes in a monoclinic unit cell (space group $P2_1/c$). As with $Sn(NH_3)_2F_4$ the $NH_3$ groups are in trans position with respect to each other. The silicon atoms are distributed on a C centered lattice, in distinction to the body centered distribution of tin in $Sn(ND_3)_2F_4$. Furthermore, the N–Si–N axis is tilted with respect to the *b*-axis of the unit cell and alternates along the *b*-axis. The hydrogen bonding system is also quite different: the three hydrogens of the ammonium group are pointing towards the fluorine atoms of three neighboring octahedral faces (Fig. 3b). This is illustrated by the Si–N–(H)–F bond angles, which are 108°, 105°, and 111°. All three are close to

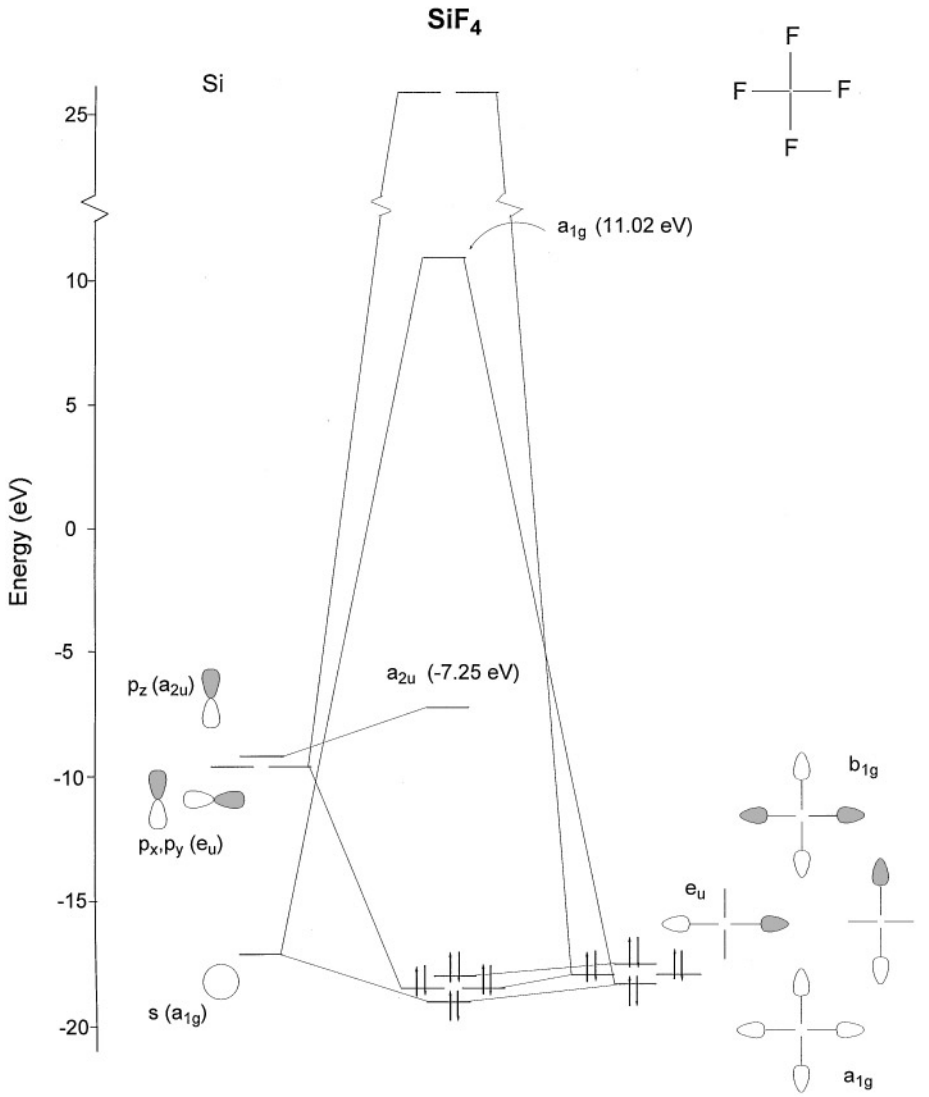


**FIG. 5.** The MO interaction diagram for the hypothetical molecule $SiF_4$. For simplicity the fluorine based orbitals, which are primarily nonbonding in character, have been omitted. The two lowest energy unoccupied orbitals of $a_{2u}$ ($-7.25$ eV) and $a_{1g}$ (11.02 eV) symmetry are shown in more detail in Fig. 7.

the ideal tetrahedral bond angle of 109.5° that would result from an ideal ammonia group with linear N–H–F bonds. This compares to Sn–N–(D)–F bond angles of 99°, 98°, 118°, and 105° for $Sn(ND_3)_2F_4$. These angles are compared because the errors in the hydrogen positions in $Si(NH_3)_2F_4$ are quite large and less reliable than those obtained for $Sn(ND_3)_2F_4$. This is due to the higher neutron scattering power of deuterium. The nitrogen–hydrogen distances in $Si(NH_3)_2F_4$ are therefore much too small. In $NH_3$ they should be approximately 0.90 Å. This error leads to unreasonable bond valence parameters for the hydrogen and nitrogen atoms. However, if we look at individual bond valences we see again the general trend that the silicon and nitrogen are overbonded and the fluorines underbonded. Even though the molecular structures are the same the crystal structures are different. This is a result of the different hydrogen bonding scheme which has to be altered if the reaction is going to proceed to complexes (IV) and (V). The two 2-center hydrogen bonds involving D(2) and D(3) are likely to be eliminated via HF extraction before D(1), which is involved in a three-center hydrogen bond. Bond valence calculations mentioned above support this view. In $Si(ND_3)_2F_4$ all three hydrogen of the ammonia group are involved in hydrogen bonding interactions with similar strengths.

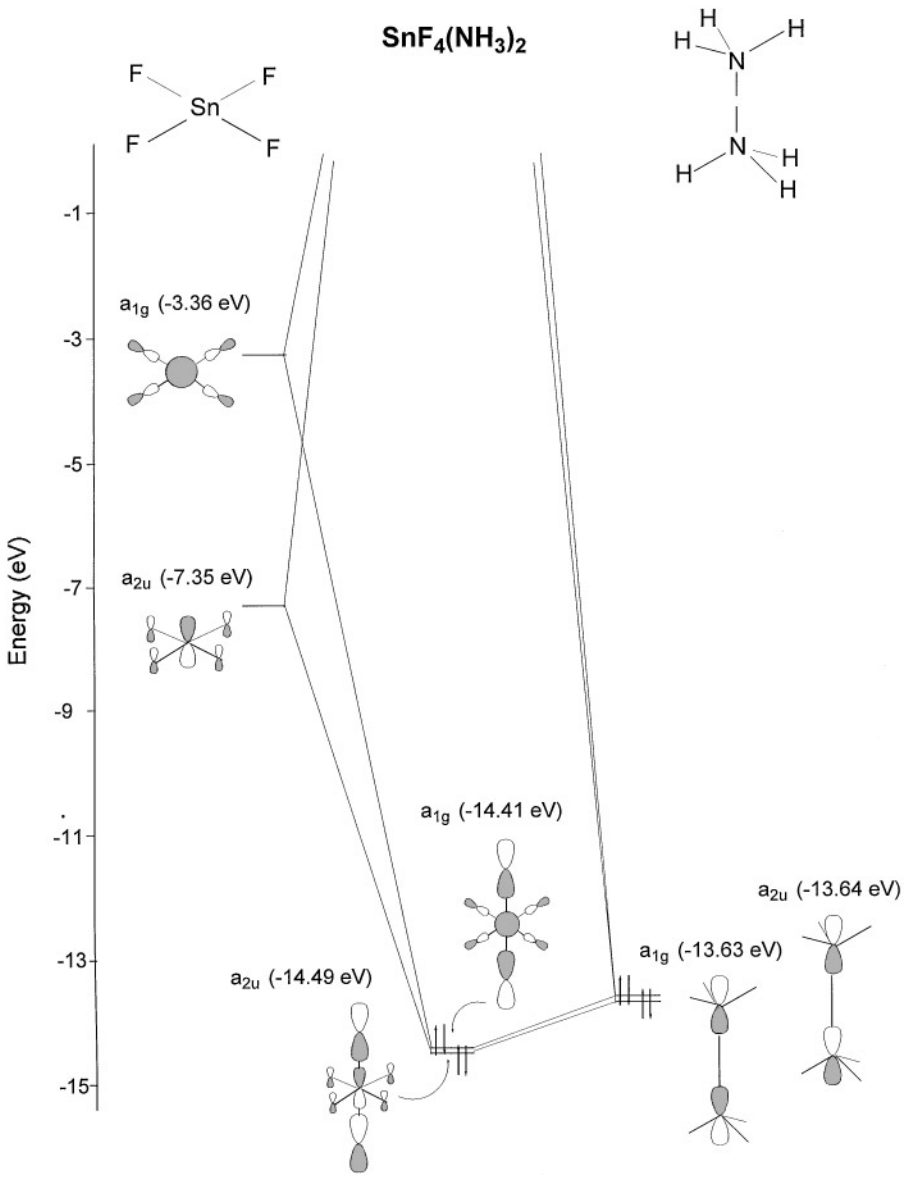


**FIG. 6.** The MO interaction diagram showing the interaction between the HOMO donor orbitals on the ammonia ligands (primarily N $p_z$ in character) and the LUMO acceptor orbitals on $SnF_4$ (shown in Fig. 4).

*Molecular Orbital Calculations*

While hydrogen bonding forces dictate the intermolecular orientation and packing of molecules, covalent bonding interactions between the central metal ion and its fluorine and nitrogen ligands are responsible for the intramolecular geometry. The relative simplicity of the molecular solids $Si(NH_3)_2F_4$ and $Sn(NH_3)_2F_4$ make molecular orbital (MO) calculations computationally feasible and relatively straightforward to interpret. The results of these calculations are invaluable in understanding the stability, reactivity and intramolecular structure of these compounds. Furthermore, the relative strength of the metal–fluorine and metal–nitrogen interactions will be important parameters in subsequent steps of the ammonolysis. In order to understand the results of the MO calculations we consider first the neutral square planar molecules $SnF_4$ and $SiF_4$ and the symmetry adapted linear combination (SALC) of two $NH_3$ ligands. The MO diagrams for these species are given in Figs. 4 and 5. Due to lack of either spatial or energetic overlap most of the MOs in Figs. 4 and 5 can be considered essentially non bonding orbitals with fluorine character. However, the empty antibonding orbitals with symmetry $a_{1g}$ and $a_{2u}$ are of proper symmetry to interact with the filled $p_z$ orbitals of the nitrogen ligands. This donor–acceptor interaction is responsible for the formation of the HOMO

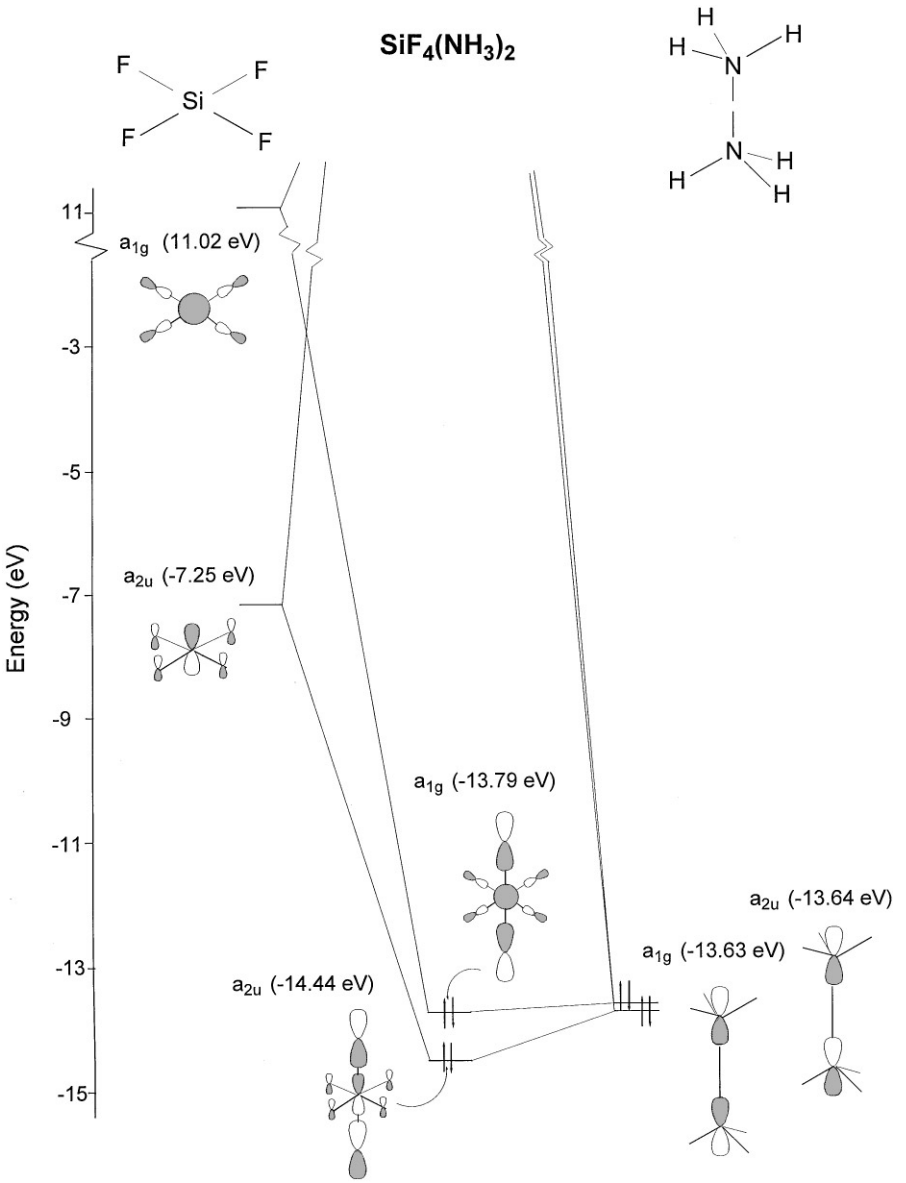


**FIG. 7.** The MO interaction diagram showing the interaction between the HOMO donor orbitals on the ammonia ligands (primarily N $p_z$ in character) and the LUMO acceptor orbitals on $SiF_4$ (shown in Fig. 5).

orbitals in both $M(NH_3)_2F_4$ complexes and is shown for $M = Sn$ and $M = Si$ in Figs. 6 and 7, respectively. The most striking difference when going from tin to silicon is that the $a_{1g}$ antibonding orbital is raised in energy from $-3.36$ to $+11.02$ eV. This is a result of the increased electronegativity (more negative $H_{ii}$, see Table 6) of the *s* orbital of silicon with respect to tin. This leads to an increase in the mixing between the silicon 3*s* orbital and the 2*p* orbitals of fluorine. This stabilization of the Si–F bonding increases the energy of the $a_{1g}$ antibonding orbital to a point where it can no longer effectively stabilize the nitrogen $p_z$-based SALC of $a_{1g}$ symmetry, because the energy separation between the two orbitals is too large. Thus the donor–acceptor interaction between the two levels is negligible and both orbitals remain essentially nonbonding in $Si(NH_3)_2F_4$. In contrast, the antibonding $a_{2u}$ level is primarily of Si $p_z$ character due to the small spatial and energetic overlap with the fluorine $p_z$ orbitals. The energy of this level, $-7.25$ eV, is sufficiently negative to stabilize the $a_{2u}$ nitrogen $p_z$ based SALC.

In the tin case significant differences in this interaction are evident as shown in Fig. 6. The $a_{2u}$ interaction energies remain quite similar to those observed for $M = Si$, but now the energy of the $a_{1g}$ $SnF_4$ antibonding level is low enough to stabilize the $a_{1g}$ nitrogen based SALC. Thus the energy of the HOMO goes from $-13.64$ eV in an isolated $NH_3$ molecules to $-14.41$ eV in $Sn(NH_3)_2F_4$. This is a consequence of the metal-based $a_{1g}$ orbital having largely tin *s* character with only a small fluorine antibonding component. This leads to an increase in the Sn–N bond overlap because both Sn *s* and $p_z$ orbitals act as acceptor levels for the lone electron pairs on the nitrogen ligands, whereas in $Si(NH_3)_2F_4$ the Si *s* orbital is involved in bonding to the fluorine and only the $p_z$ orbital is available to accept electron density from nitrogen.

## CONCLUSIONS

The results of the present MO study of $M(NH_3)_2F_4$ molecules indicate that the *M*–F bonding is stronger when $M = Si$ and the *M*–N bonding is stronger when $M = Sn$. This can be understood by looking at its various structural manifestations: at the simplest level we see that the average *M*–F and *M*–N distances vary from 1.99 Å and 2.10 Å in $Sn(NH_3)_2F_4$ to 1.67 Å and 1.90 Å in $Si(NH_3)_2F_4$. Thus upon substitution of the smaller silicon for tin the *M*–F bond contracts more than the *M*–N bond. Extending the analysis and performing bond valence calculations (16), Table 8 reveals a significant increase in the *M*–F bond valence and a substantial decrease in the *M*–N bond valence upon going from tin to silicon. Finally, the overlap populations calculated by CAESAR and also given in Table 8 show the same trend. These different aspects of the bonding in $M(NH_3)_2F_4$ all reveal that going from tin to silicon enhances the strength of the *M*–F bonds at the expense of the *M*–N bonding. This may be viewed as a consequence of classical hard–soft interactions. Compared to tin, silicon is a relatively hard cation and fluorine is the prototypical hard anion. Therefore, the Si–F hard–hard interactions and the Sn–N soft–soft interactions are energetically favored. As the ammonolysis reaction progresses the number of metal–nitrogen bonds in the compound increases at the expense of metal–fluorine bonds. A soft cation such as tin will respond to this more favorably than a harder cation such as silicon or germanium.

Based on our study of the inter- and intramolecular differences between $Si(NH_3)_2F_4$ and $Sn(NH_3)_2F_4$ we conclude that the HF extraction in the ammonolysis reaction to the one-dimensional system $M(NH_3)_2F_2$ is facilitated in the case of $Sn(NH_3)_2F_4$ by (i) a decreased metal–fluorine bond strength in the octahedral complex and (ii) a hydrogen bonding network with two different hydrogen bonding interactions.

**TABLE 8**
**Measures of the Bond Strength in $SnF_4(NH_3)_2$, and $SiF_4(NH_3)_2$**

| Bond strength parameter | $M = Si$ | $M = Sn$ |
|---|---|---|
| Average *M*–F bond distance (Å) | 1.67 | 1.99 |
| Average *M*–N bond distance (Å) | 1.90 | 2.10 |
| Average *M*–F bond valence | 0.87 | 0.67 |
| Average *M*–N bond valence | 0.63 | 0.93 |
| *M*–F overlap population | 0.33 | 0.24 |
| *M*–N overlap population | 0.32 | 0.35 |

*Note.* The bond valences were calculated using the program VALENCE (18). The overlap populations were calculated using CAESAR and are obtained by summing over all occupied molecular orbitals to calculate the quantity $\sum 2C_iC_jS_{ij}$, where $C_i$ and $C_j$ are coefficients for all valence atomic orbitals $\chi_i$ and $\chi_j$ on the respective atoms involved in the overlap, and $S_{ij}$ is the overlap integral $S_{ij} = \langle \chi_i | \chi_j \rangle$.

## ACKNOWLEDGMENTS

This work was partly supported by the Division of Materials Sciences, U.S. Department of Energy, under Contract DE-AC02-76CH00016. The authors thank Jinqing Ren and Myung-Hwan Whangbo for making the program CAESAR available prior to general release. Discussions with Dong-Kyun Seo regarding the MO calculations and the use of CAESAR were very helpful and much appreciated. John Evans (Oxford) is thanked for assistance in setting up the rigid body refinement in GSAS. Financial support for this work was received from the Deutsche Forschungsgemeinschaft and Fonds der Chemischen Industrie.

## REFERENCES

1. J. Rouxel, M. Touroux, and R. Brec (Eds.), "Soft Chemistry Routes to New Materials—Chimie Douce," Materials Science Forum, Vols. 152–153. Trans Tech Publications, Switzerland, 1994.
2. S. Andersson, *Ark. Kemi.* **26,** 521 (1967).

3. $Mg_3NF_3$, $Mg_2NF$: S. Andersson, *J. Solid State Chem.* **1,** 306 (1970). $CA_2NF$: J. Galy, M. Jaccou, and S. Andersson, *C.R. Acad. Sci. Paris* **272,** 1657 (1971). ThNF: R. Juza, R. Sievers, and W. Jung, *Naturwissenschaften* **53,** 551 (1966). TiNF: C. Wüstefeld, T. Vogt, J. Strähle, and H. Fuess, *Angew. Chem.* **100,** 1013 (1988). $Ce_3NF_6$, $Pr_3NF_6$: T. Vogt, E. Schweda, J. P. Laval, and B. Frit, *J. Solid State Chem.* **83,** 324 (1989). $Bi_3NF_6$: M. Hofmann, E. Schweda, J. Strähle, J. P. Laval, B. Frit, and M. A. Estermann, *J. Solid State Chem.* **114,** 73 (1995). $Zr_4ON_3F_5$, ZrNF: R. Schlichenmaier, E. Schweda, J. Strähle, and T. Vogt, *Z. Anorg. Allg. Chem.* **619,** 367 (1993).
4. K. M. Rabe, J. C. Phillips, P. Villars, and I. D. Brown, *Phys. Rev. B* **45,** 7650 (1992).
5. C. Plitzko and G. Meyer, *Z. Anorg. Allg. Chem.* **622,** 1646 (1996).
6. W. Weber and E. Schweda, *Z. Anorg. Allg. Chem.* **621,** 617 (1995).
7. W. Weber, Ph.D. thesis, Unviersity of Tübingen, 1996.
8. J. D. Axe, S. Cheung, D. E. Cox, L. Passell, T. Vogt, and S. Bar-Ziv, *J. Neutron Res.* **2**(3), 85 (1994).
9. A. C. Larson and R. B. Von Dreele, LANSCE, Los Alamos National Laboratory, Los Alamos, NM, 1994.
10. P. E. Werner, L. Eriksson, and M. Westdahl, *J. Appl. Crystallogr.* **18,** 367 (1985).
11. R. D. Shannon, *Acta Crystallogr. Sect. A* **32,** 751 (1976).
12. R. Hoffmann, *J. Chem. Phys.* **39,** 1397 (1963).
13. R. Hoffmann and W. N. Lipscomb, *J. Chem. Phys.* **36,** 2179 (1962).
14. R. Hoffmann and W. N. Lipscomb, *J. Chem. Phys.* **37,** 2872 (1962).
15. M. H. Whangbo and R. Hoffmann, *J. Am. Chem. Soc.* **100,** 6093 (1978).
16. T. A. Albright, J. K. Burdett, and M. -H. Whangbo, "Orbital Interactions in Chemistry," Chap. 1. Wiley, New York, 1985.
17. J. Ammeter, H. -B. Buergi, J. Thibeault, and R. Hoffmann, *J. Am. Chem. Soc.* **100,** 3686 (1978).
18. I. D. Brown, *J. Appl. Crsytallogr.* **29,** 479 (1996).
19. I. D. Brown, *in* "Structure and Bonding in Crystals, vol. 2," (M. O'Keefe and A. Navrotsky Eds.), pp. 1–30. Academic Press, New York, 1981.